PIMC Simulations of Metal Hydrogen: Phase Transition and Equation of State

Alexander Novoselov† *, Oleg Pavlovsky† ‡, Maxim Ulybyshev† ‡

† *Moscow State University, Moscow, Russia*

‡ *Institute for Theoretical and Experimental Physics, Moscow, Russia*

∗ *E-mail: novoselov@goa.bog.msu.ru*

Abstract

The article is devoted to numerical studies of atomic (metal) hydrogen with Path Integral Monte Carlo (PIMC) technique. The research is focused on the range of temperatures and densities where quantum statistics effects are crucial for electrons and negligible for protons. In this range the equations of state are obtained as a dependence of internal energy and pressure on temperature and density. These dependences allow to detect and describe the phase transition between solid and liquid phases.

1 Introduction

One of the major recent achievements of astrophysics is the discovery of numerous exoplanetary systems. Almost thousand such planets have been discovered [1]. Most of them are gas giants up to ten Jovian masses. That is the reason that attracts an increasing interest to the models of planetary evolution. By the current conception gas giants mainly consist of hydrogen and helium. So the equation of state of these elements is crucial for the models of planetary formation and evolution.

The detection of huge magnetic moment of the solar system gas giants has proven that they have liquid metal hydrogen core [2]. There are some exoplanets that are much more massive and maybe colder than Jupiter. Because of higher pressure and less temperature their cores may contain not only liquid, but also solid crystal hydrogen. The formation, evolution and properties of planets are determined by the balance of gravity and pressure, and the pressure in one's turn is determined by the equation of state and thermodynamical parameters of the planetary matter. In the cores of gas giants the prevailing substance is metal hydrogen. It can be described as a many-body quantum system. Its analytic analysis is extremely complicated, so the numerical calculations are actual in this problem.

This article is devoted to Path Integral Monte Carlo simulation of metal hydrogen. In the explored range of temperatures and densities electrons form a degenerate quantum gas while nuclei can be examined with classical statistics, that allows to avoid fermion statistics problem. The parameters to be explored are internal energy and pressure and their dependence on temperature and density. We also focus on the phase transition between liquid and crystal phases. It is detected and explored in a wide range of densities.

It should be noted that the study of metal hydrogen is important not only for astrophysics, but also due to the progress in diamond anvil cell experiments that have recently obtained crystal metal hydrogen in the laboratory [3].

We broadly use nuclear units in this work: $k_e = \hbar = e = m_p = 1$; here k_e is Coulomb constant and m_p is proton mass. Corresponding units of principal physical quantities are: nuclear Bohr radius $a_{0N} = L_N = 2.9 \times 10^{-14}$ m for length, nuclear Hartree $Ha = E_N =$

8.0×10^{-15} J for energy, $p_N = 3.3 \times 10^{26}$ Pa for pressure unit, $\rho_N = 7.0 \times 10^{13}$ kg/m^3 for density unit and $T_N = 5.8 \times 10^8$ K for temperature unit. In nuclear units electron mass is $m_e = 5.4 \times 10^{-4}$ and (electron) Bohr radius is $a_{0e} = 1/m_e = 1.8 \times 10^3$.

We study the dependence of the atomic hydrogen properties on temperature and density, described by parameters β

$$\beta = 1/k_B T \tag{1}$$

and r_s (Wigner-Seitz radius)

$$\rho = \frac{m}{\frac{4}{3}\pi r_s^3} \tag{2}$$

respectively. We simulate a finite cell of the substance, containing $N_p = 128$ particles. The properties to be evaluated in the simulation are internal energy (the sum of kinetic and potential energies of the particles)

$$E = K + V \tag{3}$$

and pressure P. It is well known that the functions $E(\rho, T)$ and $P(\rho, T)$ provide a complete thermodynamical description of the system. In order to obtain an obvious measure of the order of the system we also calculate Lindemann ratio

$$\mathcal{L} = \frac{\sqrt{\langle x^2 \rangle}}{R_n}. \tag{4}$$

Here $\langle x^2 \rangle$ is the particle displacement from its site in crystal lattice and R_n is the distance to the nearest neighbouring particle. Lindemann ratio is used to explicitly distinguish chaotic and crystal phase.

2 Model

The Hamiltonian of atomic hydrogen is

$$H_{full} = K_N + K_e + V_0 + V_e + V_{int}. \tag{5}$$

Here K_N and K_e are kinetic energies of nuclei (protons) and electrons respectively. V_0, V_e and V_{int} are potential energies of nuclei-nuclei, electron-electron and nuclei-electron interaction respectively; all three are sums of pair Coulomb interaction, for example

$$V_0 = \sum_{i_1=1}^{N_p} \sum_{i_2=1}^{i_1-1} \frac{1}{r_{i_1 i_2}}. \tag{6}$$

There is a wide range of temperatures and densities where on the one hand electrons can be considered as degenerate Fermi gas and Tomas-Fermi model is applicable to them (i. e. Fermi statistics is of primary importance), but on the other hand protons are strongly not degenerate and their statistics is of no importance. On these assumptions we can deal only with protons, moreover we can use classical (Botzmann) statistics. The effect of taking electrons into account is Thomas-Fermi screening. So the effective Hamiltonian is

$$H_{full} = K_N + V_N. \tag{7}$$

Here V_N is potential energy of protons with screened interaction:

$$V_N = \sum_{i_1=1}^{N_p} \sum_{i_2=1}^{i_1-1} \frac{\exp\{-r_{i_1 i_2}/R_{TF}\}}{r_{i_1 i_2}}. \tag{8}$$

Thomas-Fermi screening length R_{TF} is given by

$$R_{TF} = \sqrt[3]{\frac{\pi}{12}}\sqrt{a_{0e}r_s}. \tag{9}$$

The Hamiltonian (5) can be reduced to (7) under following conditions. First, we want to neglect effects of nuclear forces for protons, so their separation (which is approximately r_s) must me much greater than their size R_p. Second, we want to applicate Thomas-Fermi theory to electrons, that can be done if there are many electrons within screening length. This leads intuitively obvious restriction that nuclei separation must me less than (electron) Bohr radius. So, our approximation are applicable for densities corresponding

$$R_p \ll r_s \ll a_{0e}. \tag{10}$$

The limits in nuclear and SI units are $R_p \approx 3 \times 10^{-2} \approx 9 \times 10^{-16}$ m and $a_{0e} \approx 2 \times 10^3 \approx 5 \times 10^{-11}$ m. The estimations for limiting densities (2) are $\rho_{min} \approx 3 \times 10^3$ kg/m^3 and $\rho_{max} \approx 6 \times 10^{17}$ kg/m^3.

Next, our approximation is valid if electrons are degenerate and protons are not. The degeneracy temperature can be estimated as $\beta_d \approx mr_s^2$. So, the acceptable range of temperatures depends on density and it is defined as

$$m_e r_s^2 \ll \beta \ll r_s^2. \tag{11}$$

The temperature limits in nuclear units are $\beta_{min} \approx 5 \times 10^{-4}\ r_s^2$ and $\beta_{max} \approx r_s^2$. This leads following estimations at given densities (in SI units): $T_{min} \approx 0.9\rho^{\frac{2}{3}}\mathrm{kg}^{-2/3}\mathrm{m}^2\mathrm{K}$ and $T_{max} \approx 2 \times 10^5\rho^{\frac{2}{3}}\mathrm{kg}^{-2/3}\mathrm{m}^2\mathrm{K}$.

3 PIMC

3.1 Path Integral Monte Carlo

Suppose a system, determined by coordinates $\mathbf{x}$, in imaginary time. The density matrix of such system with Hamiltonian H at the temperature β is

$$\rho_{x_0 \to x_{N_t}} = \langle \mathbf{x}_0 | e^{-\beta H} | \mathbf{x}_{N_t} \rangle. \tag{12}$$

Its partition function is

$$Z = \mathrm{tr}\rho = \int d\mathbf{x_0} \langle \mathbf{x}_0 | e^{-\beta H} | \mathbf{x}_0 \rangle. \tag{13}$$

Average observable A is calculated with

$$\langle A \rangle = \frac{1}{Z}\mathrm{tr}(A\rho) = \frac{1}{Z}\int d\mathbf{x}_0 \langle \mathbf{x}_0 | A e^{-\beta H} | \mathbf{x}_0 \rangle. \tag{14}$$

To proceed to the path integral formulation, introduce the "time step" τ, defined as

$$1/T = \beta = N_t \tau. \tag{15}$$

and decompose the density matrix into a product of N_t density matrices

$$\rho_{x_0 \to x_{N_t}} = \rho_{x_0 \to x_1} \cdots \rho_{x_{t-1} \to x_t} \cdots \rho_{x_{N_t - 1} \to x_{N_t}}, \tag{16}$$

where each of these intermediate matrices is

$$\rho_{x_{t-1}\to x_t} = \langle \mathbf{x}_{t-1}|e^{-\tau H}|\mathbf{x}_t\rangle \equiv e^{-S_t}. \tag{17}$$

"Lattice action" S is defined as

$$S = \sum_{t=1}^{N_t} S_t. \tag{18}$$

In fact the above decomposition given by Trotter formula is correct only if $N_t \to \infty$, and for real simulation N_t will be chosen large enough to eliminate the dependence of the result on it. Next we introduce the notation

$$\mathcal{D}\mathbf{x} = \prod_{t=1}^{N_t} d\mathbf{x}_t \tag{19}$$

and consequently the formulae (13) and (14) can be represented as follows:

$$Z = \int \mathcal{D}\mathbf{x} e^{-S}, \tag{20}$$

$$\langle A\rangle = \frac{\int \mathcal{D}\mathbf{x} A e^{-S}}{\int \mathcal{D}\mathbf{x} e^{-S}} = \int A \frac{\mathcal{D}\mathbf{x} e^{-S}}{\int \mathcal{D}\mathbf{x} e^{-S}} \tag{21}$$

Formula (21) reveals the idea of Path Integral Monte Carlo. Since we have a (large enough) set of paths $x = \mathbf{x}_0 \dots \mathbf{x}_t \dots \mathbf{x}_{N_t}$, where the probability of the path to be included into the set is proportional to its "statistical weight"

$$\pi(x) \sim e^{-S(x)}. \tag{22}$$

The average of any observable can be measured by simple (arithmetic) averaging over this set.

3.2 Algorithms

The way to obtain properly distributed (22) paths is based on the property of Markov chains to converge to the limiting distribution. A sufficient condition of the convergence to the limiting distribution $\pi(x)$ for the Markov chain with a transition probability $\mathcal{P}(x \to x')$ is the detailed balance condition:

$$\mathcal{P}(x \to x')\pi(x) = \mathcal{P}(x' \to x)\pi(x'). \tag{23}$$

The specific form of $\mathcal{P}(x \to x')$ is not fixed, but it must be constructed carefully as it crucially affects the time of "thermalization" (convergence to the limiting distribution).

A generalized Metropolis-Hastings algorithm is based on the decomposition of transition probability:

$$\mathcal{P}(x \to x') = \mathcal{T}(x \to x')\mathcal{A}(x \to x') + \delta(x - x')\left\{1 - \int dy \mathcal{T}(x \to y)\mathcal{A}(x \to y)\right\}, \tag{24}$$

here

$$\mathcal{A}(x \to x') = \min\left[1, \frac{\mathcal{T}(x' \to x)\pi(x')}{\mathcal{T}(x \to x')\pi(x)}\right]. \tag{25}$$

It satisfies the detailed balance condition for any $\mathcal{T}(x \to x')$. Formula (25) means the following. First, generate a new (trial) configuration with probability $\mathcal{T}$; then accept it (add it to the set) with probability $\mathcal{A}$ or reject it (return to the previous configuration and add an other copy of

it to the set) with probability $1-\mathcal{A}$. The specific form of the algorithm is defined by the choice of the function $\mathcal{T}(x \to x')$. The theoretically best choice is "heat bath":

$$\mathcal{T}(x \to x') = \pi(x'),\ \mathcal{A}(x \to x') = 1,\ \mathcal{P}(x \to x') = \pi(x'). \tag{26}$$

Unfortunately, most probability distributions can not be generated directly fast enough, so we have to use a general type of the algorithm (25). There are two demands to the distribution $\mathcal{T}(x \to x')$: first, it must be close to $\pi(x')$, second, there must be an algorithm of generating it numerically very fast. It is rather natural to choose $\mathcal{T}(x \to x')$ as the kinetic part of the "statistical weight", then the acceptance probability $\mathcal{A}(x \to x')$ is proportional to its potential part.

Primitive algorithm is based on "sweep" when the transition from "old" configuration to "new" one is a try to change only one coordinate (or coordinates in the only imaginary time slice t). For large systems and for large number of slices it has huge autocorrelation. It means that "new" configurations turn out to look like "old", and it takes much time to obtain really statistically independent ones. This problem can be solved with the multilevel algorithm [4]. It is based on fast generation of a rough approximation of the path, that increase the acceptance rate of the further more accurate one.

Consider a bisection multilevel algorithm. We start from a part of the path with length $2^{N_{level}}$ slices, for example $s = (\mathbf{x}_0, \ldots, \mathbf{x}_{2^{N_{level}}})$. This part of the path is divided into levels s_k. Zero level consists of the coordinates on the boundaries of the chosen part of the pass: $s_0 = (\mathbf{x}_0, \mathbf{x}_{2^{N_{level}}})$. They are not to be changed during the current multilevel update. The first level consist of the coordinates on one middle time slice $s_1 = (\mathbf{x}_{2^{N_{level}-1}})$. The second level consist of two time slices $s_2 = (\mathbf{x}_{2^{N_{level}-2}}, \mathbf{x}_{2^{N_{level}-1}+2^{N_{level}-2}})$, etc. There are 2^{k-1} slices in the k-th level. Introduce "level action" $\pi_k(s_k) \equiv \pi_k(s_0, \ldots, s_{k-1}, s_k)$, which is a function of s_k and previous levels coordinates are parameters. Intermediate levels actions can be chosen arbitrary, the only requirement is that the action of the last level must be the lattice action:

$$\pi_{N_{level}}(s_{N_{level}}) = \pi(s). \tag{27}$$

Then start a kind of Metropolis-Hastings algorithm with trial probability distribution

$$\mathcal{T}_k(s'_k) = \mathcal{T}_k(s'_0, \ldots, s'_{k-1}; s_k; s_{k+1}, \ldots, s_{N_{level}} \to s'_0, \ldots, s'_{k-1}; s'_k; s_{k+1}, \ldots, s_{N_{level}})$$

and acceptance probability

$$\begin{aligned}\mathcal{A}_k(s'_k) = \mathcal{A}(s'_0, \ldots, s'_{k-1}; s_k; s_{k+1}, \ldots, s_{N_{level}} \to s'_0, \ldots, s'_{k-1}; s'_k; s_{k+1}, \ldots, s_{N_{level}}) = \\ = \min\left[1, \frac{\mathcal{T}_k(s_k)\pi_k(s'_k)\pi_{k-1}(s_k)}{\mathcal{T}_k(s'_k)\pi_k(s_k)\pi_{k-1}(s'_k)}\right].\end{aligned} \tag{28}$$

It satisfies the level detailed balance condition

$$\mathcal{P}_k(s'_k)\frac{\pi_k(s_k)}{\pi_{k-1}(s_{k-1})} = \mathcal{P}_k(s_k)\frac{\pi_k(s'_k)}{\pi_{k-1}(s'_{k-1})} \tag{29}$$

that leads to full detailed balance (23):

$$\pi_k(s_k) = \int ds_{k+1} \ldots ds_{N_{level}} \pi(s). \tag{30}$$

3.3 Some Details

Our simulation is limited in the number of particles, and consequently in the spatial size of the cell. We use cubic cell and periodic boundary conditions in space. The size of the cell is

$$L = \sqrt[3]{\frac{4}{3}\pi N}\ r_s. \tag{31}$$

The $\alpha = x, y, z$ coordinate of i-th particle in the t-th time slice is denoted by $x_i^\alpha(t)$. To describe the configuration completely we also need "winding numbers" $n_i^\alpha(t) = -1, 0, 1$, that denote if the corresponding path "skips" from one side of the cell to another through periodic spatial boundary conditions. Potential energy of particle interaction (particles can be in different "copies" of the cell due to boundary conditions) is determined by their separation

$$r_{i_1 i_2}^{n^1 n^2 n^3}(t) = \sqrt{\sum_{\alpha=1}^{3} (x_{i1}^\alpha(t) - x_{i2}^\alpha(t) + L n^\alpha)^2}. \tag{32}$$

In the notation, described above, the lattice action corresponding to the Hamiltonian (7) with potential energy (8) and periodic spatial boundary conditions is set as

$$-\ln\pi = S = S_T + S_V. \tag{33}$$

$$S_T = \sum_{t=1}^{N_t} \sum_{i=1}^{N_p} \sum_{\alpha=1}^{3} \frac{(x_i^\alpha(t) - x_i^\alpha(t-1) + L n_i^\alpha(t))^2}{2\tau}, \tag{34}$$

$$S_V = \sum_{t=1}^{N_t} \sum_{i_1=1}^{N_p} \sum_{i_2=1}^{i_1} \sum_{n_{i_1 i_2}^{1,2,3}(t)=-1}^{1} \frac{\exp\{-r_{i_1 i_2}^{n^1 n^2 n^3}(t)/R_{TF}\}}{r_{i_1 i_2}^{n^1 n^2 n^3}(t)} \tau. \tag{35}$$

In the case of periodic boundary conditions the trial probability density based on the kinetic part of the action can be represented as (skipping irrelevant indices for simplicity)

$$\mathcal{T}(x^\infty(t)|n(t+1) - n(t)) \sim \exp\left\{ -\frac{1}{\tau} \left[x^\infty(t) - \frac{x(t+1) + x(t-1) + L(n(t+1) - n(t))}{2} \right]^2 \right\}. \tag{36}$$

Gaussian (it has infinite range) distribution of $x^\infty(t) \equiv x'(t) + L n'(t)$ can be generated fast (we use Box-Muller transform) and allows to determine $n'(t)$, $n'(t+1)$ and $x'(t)$ due to conditions $-L/2 < x'(t) < L/2$ and $n'(t+1) - n'(t) = n(t+1) - n(t)$.

We use multilevel algorithm. Though the level action can be chosen arbitrary, there is a theoretically optimal choice. The action of the level should be obtained by integrating out the next levels coordinates in the full lattice action:

$$\pi_k(s_k) = \int ds_{k+1} \dots ds_{N_{level}} \pi(s). \tag{37}$$

For our model with action (33),(34),(35) it leads to a quite simple and effective algorithm. Trial probability distribution for each bisection is (36), where the level time step is $\tau \to \tau_k = 2^{N_{level}-k}\tau$ and winding number conserves $n_k(t+1) - n_k(t) = n_{k-1}(t)$. This trial distribution together with the condition (37) leads to the acceptance probability

$$\mathcal{A}_k(s'_k) = \min\left[1, \frac{e^{-S_V(s'_k)}}{e^{-S_V(s_k)}}\right], \tag{38}$$

$S_V(s_k)$ is determined by (35) with the first sum only over the slices that belong to the level s_k. τ is not level time step (as it was in the kinetic part) but the real time step.

4 Results

The calculations were performed for following parameters. $Na = 1/\beta$ from 0.5×10^{-5} to 4.75×10^{-5} with step 0.25×10^{-5} and for additional points 0.57×10^{-5} and 0.66×10^{-5}. r_s was changed from 200 to 450 with step 50. These values in nuclear units correspond to SI values of temperature from 2.9×10^3 K to 27.7×10^3 K and density from 183×10^3 kg/m^3 to 2085×10^3 kg/m^3. The lattice of calculation points will be shown in Figure 16 (discussed later).

4.1 Energy

Average internal energy $\langle E \rangle$ is calculated as (3), taking into account (15),(34),(35):

$$\langle V \rangle = \langle \frac{S_V}{\beta} \rangle, \tag{39}$$

$$\langle K \rangle = \langle \frac{3N_p}{2\tau} - \frac{S_T}{\beta} \rangle. \tag{40}$$

Note that while the potential energy observable is rather intuitive, the kinetic energy one is quite different from intuitive (but incorrect) form. By the way in real numerical calculations the averaging should be done exactly as in (40). $\langle T \rangle = 3N_p/2\tau - \langle S_T \rangle/\beta$ seems similar but leads to large errors because of substraction of very close large numbers.

Figures 1 and 2 show the internal energy E as a function of temperature for the densities 183×10^3 kg/m^3 and 2085×10^3 kg/m^3 respectively. In both cases we observe a slight increase with increasing temperature and an acute jump at certain temperature that is associated with the phase transition. Figures 3 and 4 show the potential energy at these densities, which behaves similar to full energy, i. e. increases and has a jump up at the same temperatures for each given density. Figures 5 and 6 show the kinetic energy at these densities. Its behaviour is different from potential and full energy. It also increases, but jumps *down* at phase transition. At lower densities this jump vanishes and turns into a jump of the slope only. So, it looks like a second-order phase transition at densities 261×10^3 kg/m^3 and lower and like a first order phase transition at densities 618×10^3 kg/m^3 and higher.

We can see that the properties of the system depend on density much stronger than on temperature. Correspondingly, the internal energy almost totally consist of potential energy determined by the distance between protons i. e. by density. In spite of this fact, the jumps of both parts of energy at the phase transition are of close magnitudes. In order to extract the main term we introduce V_{0K} - potential energy of "ideal zero temperature" crystal. It means that the particles in this crystal are exactly in the sites of its bcc (body-centric cubic) lattice (in all time slices). V_{0K} depends only on density and this dependence is shown in the Figure 7. We substract this zero energy from full and potential energy in order to extract non-trivial terms. It turns out that substracted full and potential energy and kinetic energy are of the same magnitude; their dependences on density and temperature also have close magnitudes. The substracted full internal, substracted potential and kinetic energies for a range of densities between 183×10^3 kg/m^3 and 2085×10^3 kg/m^3 are shown in figures 8, 9 and 10 respectively.

4.2 Pressure. Equation of state

The observable for pressure is

$$\langle P \rangle = \frac{2}{3L^3} \left(\langle K \rangle - \frac{1}{2} \langle \sum_{i<j} \frac{\partial V}{\partial \mathbf{r}_{ij}} \mathbf{r}_{ij} \rangle \right). \tag{41}$$

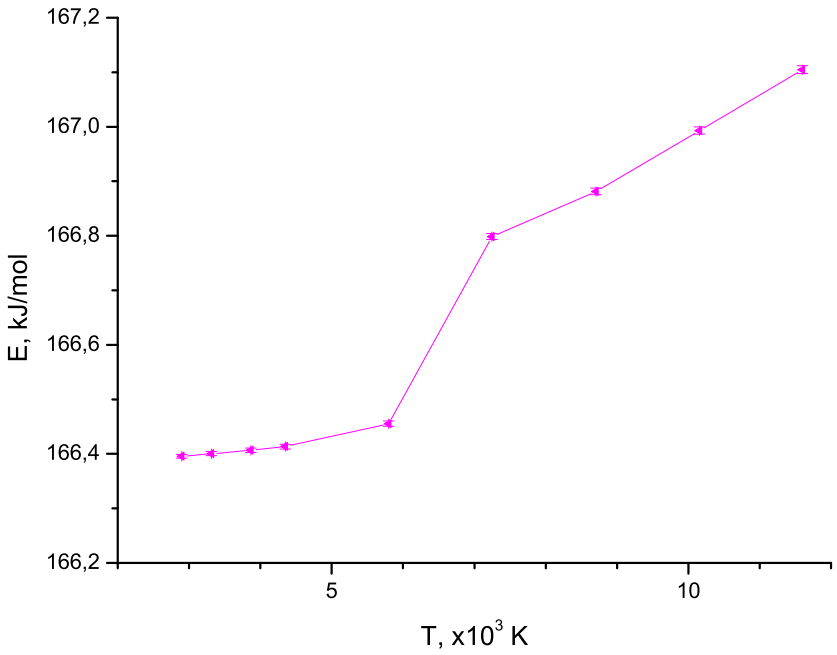

Figure 1: $E(T)$ at $\rho = 183 \times 10^3$ kg/m^3 ($r_s = 450$)

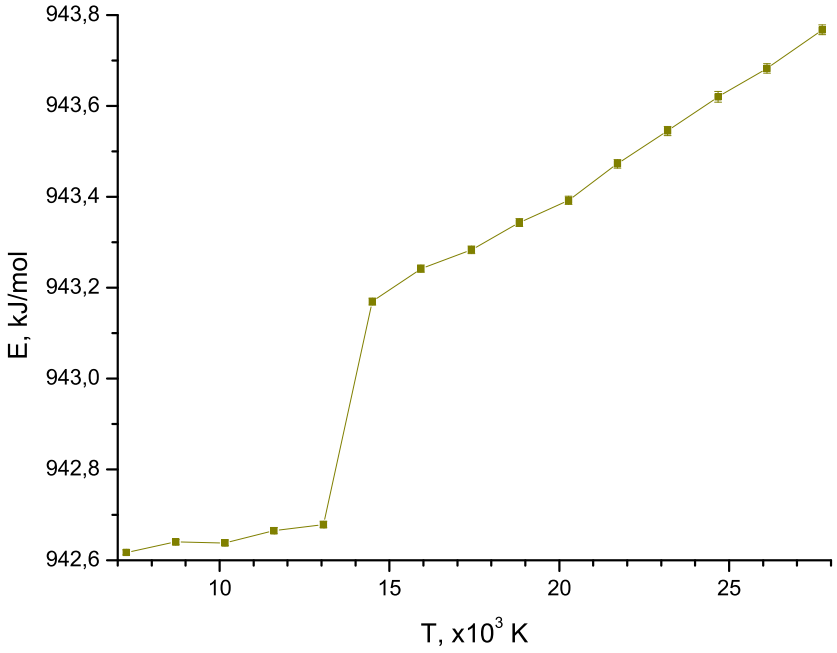

Figure 2: $E(T)$ at $\rho = 2085 \times 10^3$ kg/m^3 ($r_s = 200$)

Figures 11 and 12 show the temperature dependence of pressure at above mentioned densities. It has a jump at the same temperatures as energy that proves the existence of phase

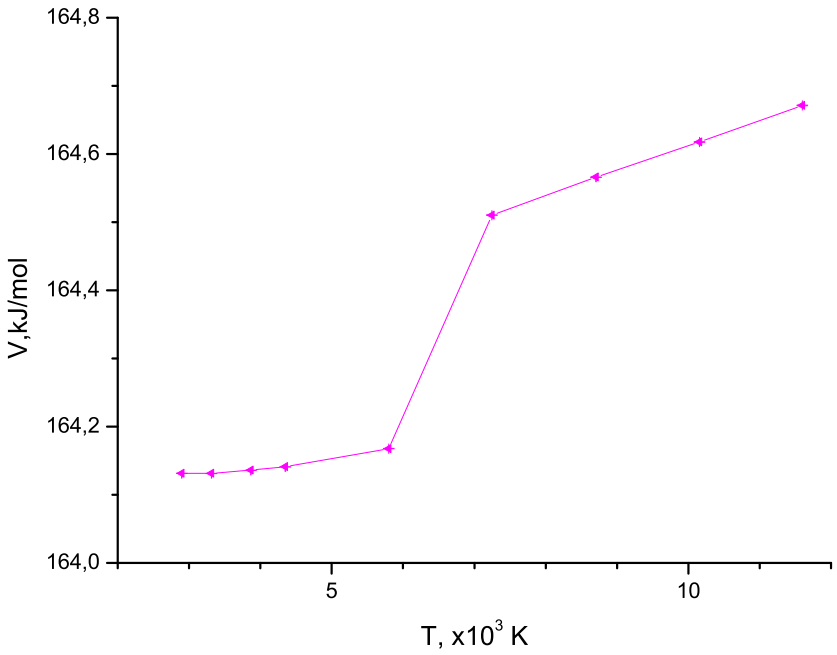

Figure 3: $V(T)$ at $\rho = 183 \times 10^3$ kg/m^3 ($r_s = 450$)

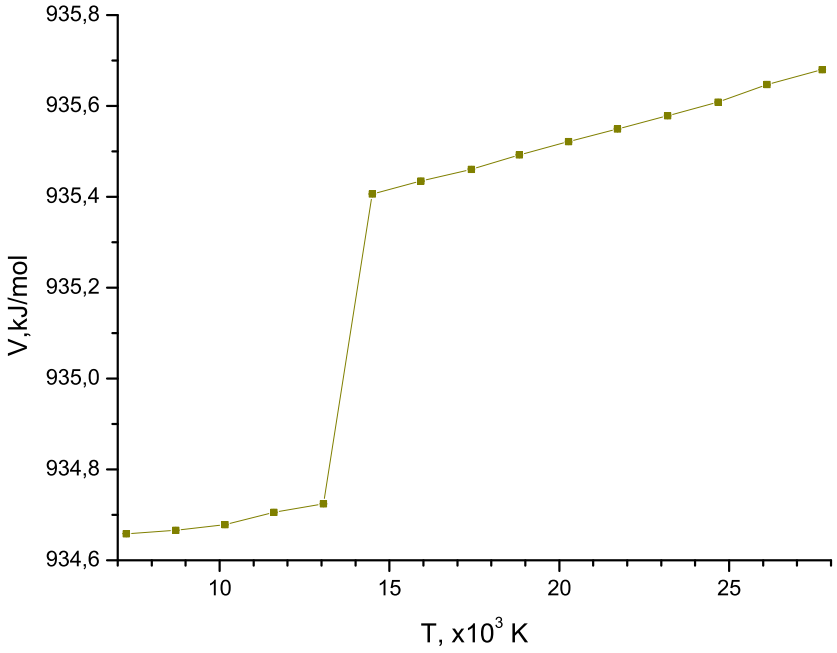

Figure 4: $V(T)$ at $\rho = 2085 \times 10^3$ kg/m^3 ($r_s = 200$)

transition. The expression (41) allows to determine P_{0K} similar to V_{0K} and perform similar substraction procedure. Figure (13) shows the dependence of P_{0K} on density and Figure 14 shows

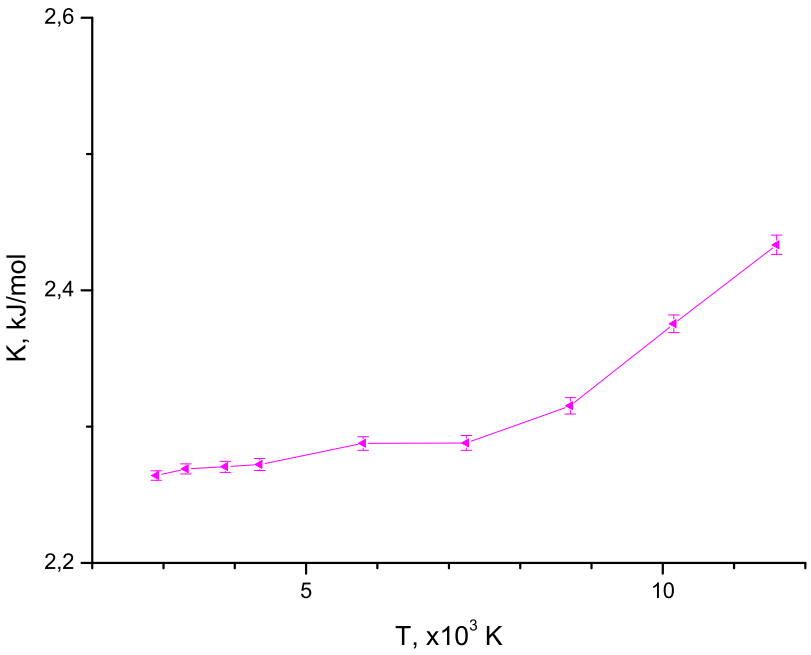

Figure 5: $K(T)$ at $\rho = 183 \times 10^3$ kg/m^3 ($r_s = 450$)

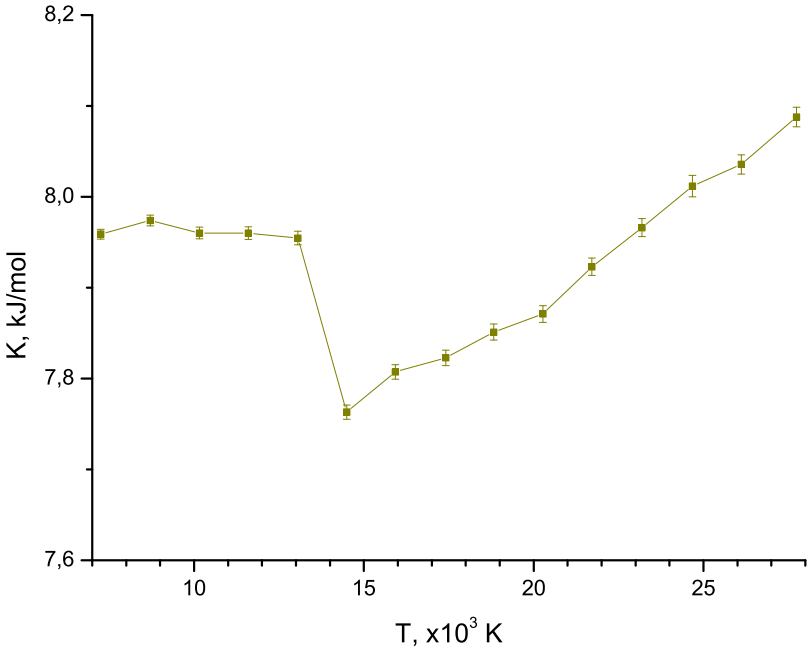

Figure 6: $K(T)$ at $\rho = 2085 \times 10^3$ kg/m^3 ($r_s = 200$)

the substracted pressure for all the range of explored densities. Similar to energy, pressure mainly depends on density and quite slightly changes with temperature. In fact it is just what

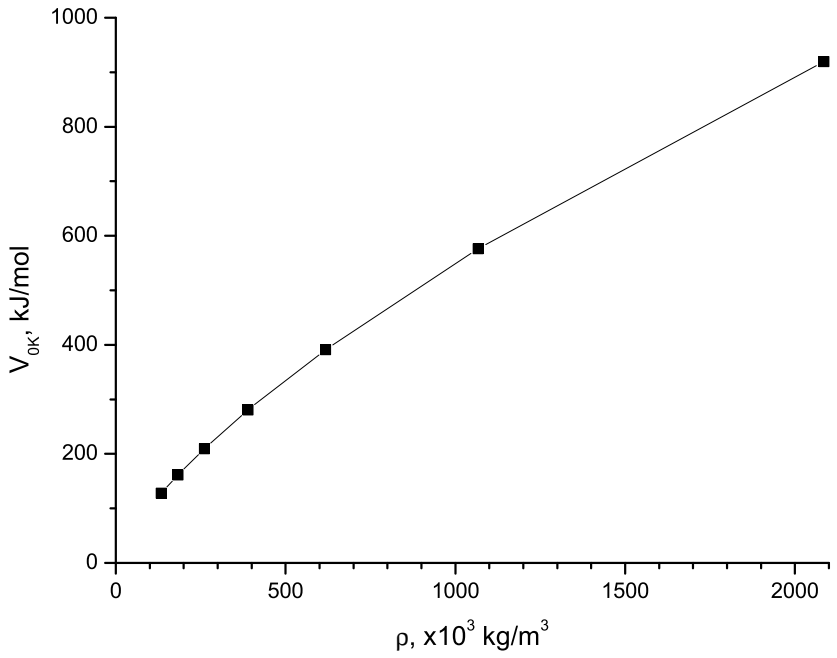

Figure 7: $V_{0K}(\rho)$

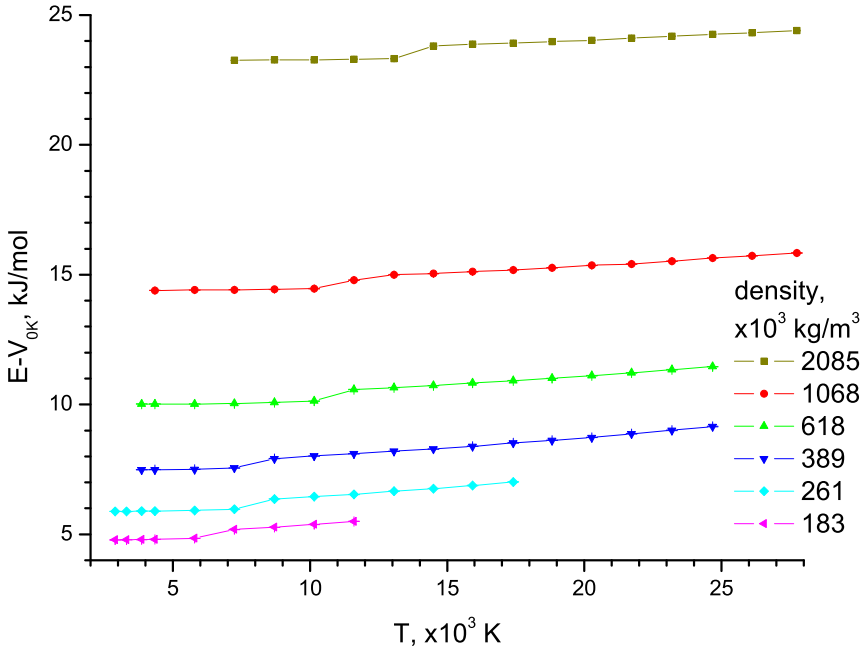

Figure 8: $E(T) - V_{0K}$ at different densities

should be expected for condensed matter. The disadvantage of this property is a trouble with thermodynamical calculations due to orders of magnitude difference between partial derivatives

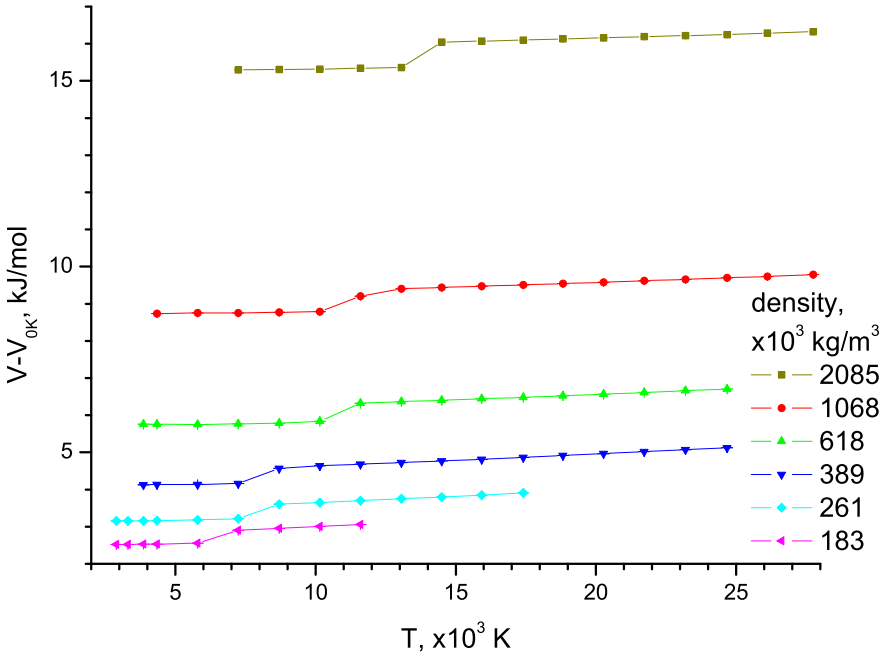

Figure 9: $V(T) - V_{0K}$ at different densities

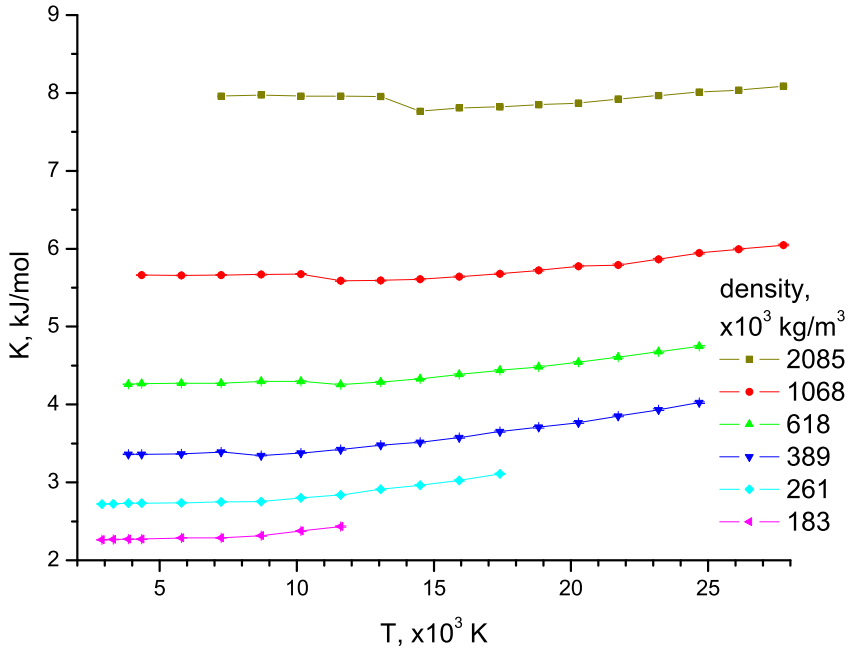

Figure 10: $K(T)$ at different densities

by density and by temperature. An intuitive illustration can be seen in Figure 14. Formally the function $P(\rho, T)$ allows to determine isobars, but the resolution of experimental data is

insufficient despite of quite large number of points. We can only say that isobars are some lines close to lines of constant density, but having some little unknown slope. This problems can be solved in different ways, but they are not to be discussed here.

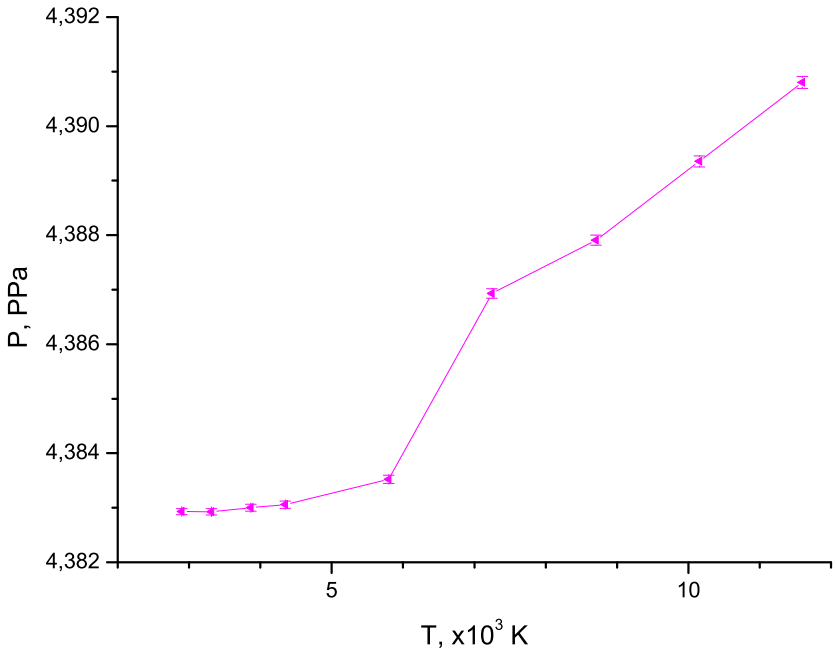

Figure 11: $P(T)$ at $\rho = 183 \times 10^3$ kg/m^3 ($r_s = 450$)

4.3 Phase transition

The Lindemann ratio (4) is a good measure of disorder of the lattice, so it is extremely useful and obvious to detect the phase transition, where the order totally vanishes. Figure 15 shows Lindemann ratio for all the range of explored densities and temperatures. The phase transition is clearly seen here. Note that while the plateau in solid phase (left bottom) gives some physical information, the plateau in liquid phase (right top) is due to finite volume effects and it is determined only by the volume.

The position of the phase transition is determined quite accurate, so we can draw the phase plane for metal hydrogen. It it shown in the Figure 16.

Here we have to describe some important details. As we know, the PIMC observables are averages over a set of thermalized path. To get this set we start with any path and perform a Markov chain procedure called thermalization. Sometime we start to get thermal equilibrium paths, but we do not know how soon it will be. It is well known that models of systems near a phase transition are usually difficult to be thermalized over the transition. For example we start our simulation with ideal "zero temperature" crystal lattice (solid state). During the calculations it thermalizes quite fast to some other solid state that seems stable. It takes quite much calculation time to receive true physical paths. An example is shown in Figure 17. This is the main obstacle to determine the position of the phase transition more accurate. Moreover, it turns out that thermalization from liquid to solid state takes so much time that it hardly ever can be performed in moderate time. So, the position of the phase transition is formally the

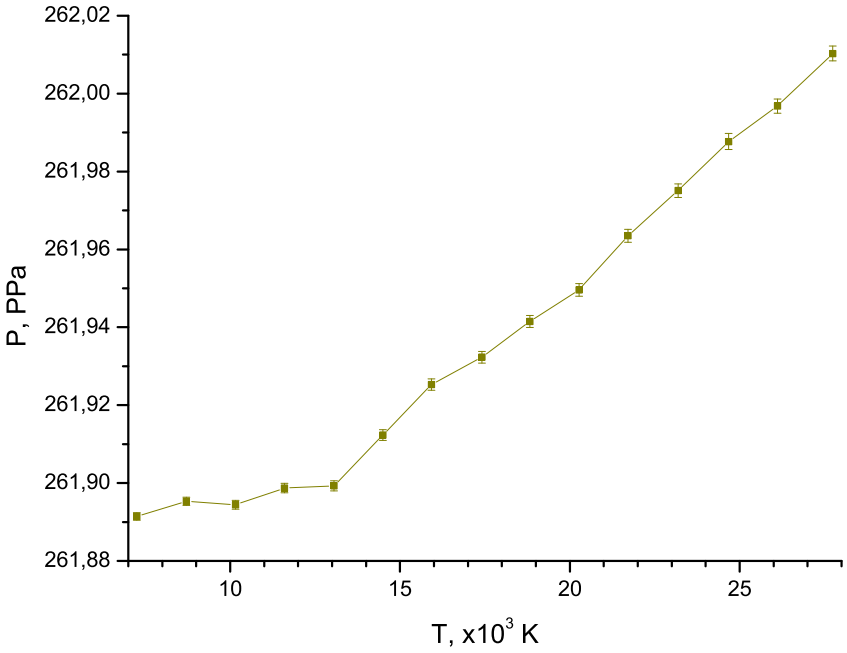

Figure 12: $P(T)$ at $\rho = 2085 \times 10^3$ kg/m^3 ($r_s = 200$)

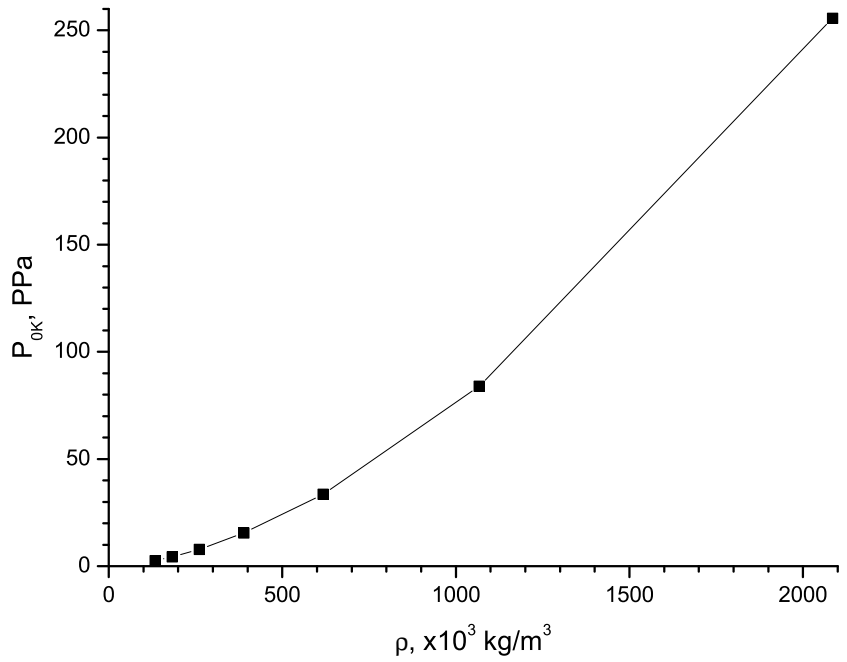

Figure 13: $P(T)$ at different densities

upper limit. The lower limit must formally be determined with a series of simulations starting from "liquid" path. But it is not expected to differ much from the upper limit that we received.

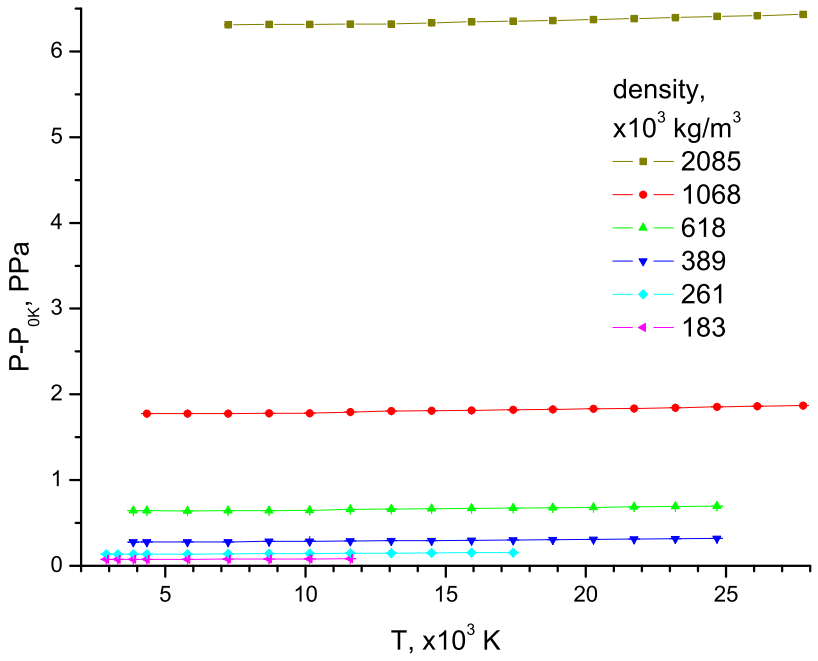

Figure 14: $P(T) - P_{0K}$ at different densities

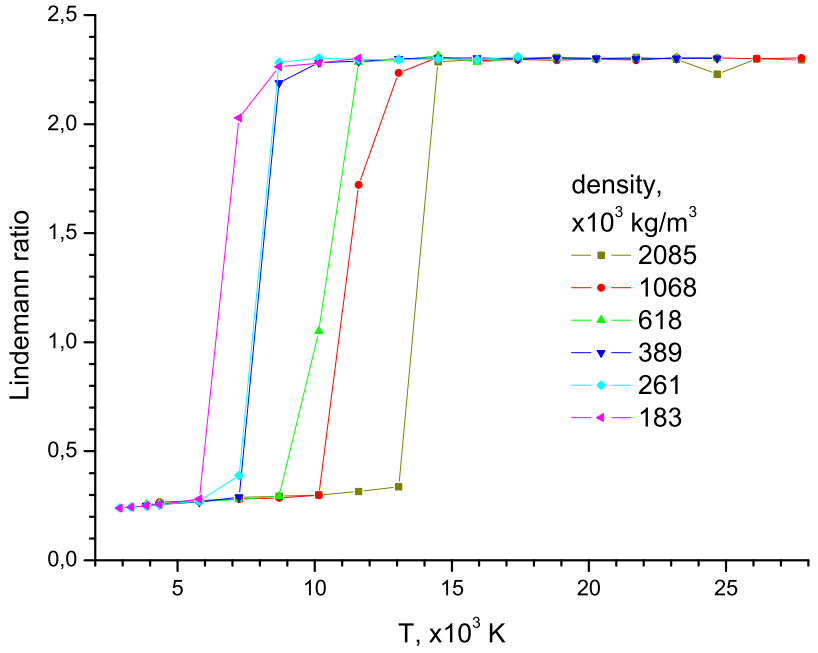

Figure 15: Lindemann ratio at different densities

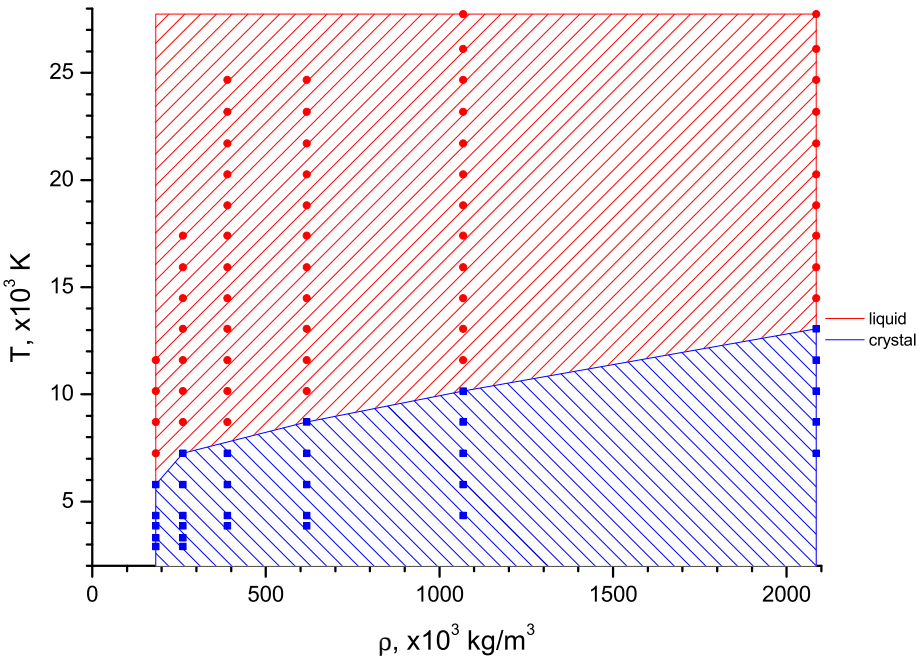

Figure 16: Phase plane

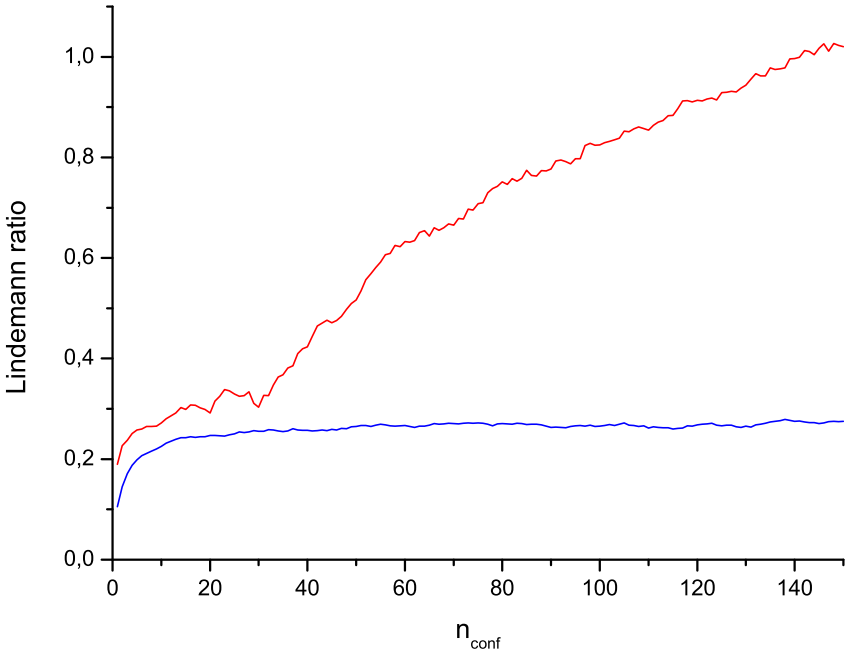

Figure 17: Lindemann ratio thermalization at $\rho = 2085 \times 10^3$ kg/m^3, $T = 13.1$ kK (blue) and $T = 14.5$ kK (red)

5 Conclusions

Path integral Monte Carlo technique was implemented to simulate atomic metal hydrogen from the first principles. Its thermodynamical properties were explored in a wide area of the phase plane. Numerical equations of state were obtained. The phase transition between liquid and solid crystal phases was detected and explored.

The principal thermodynamic parameters: temperature, density, pressure and energy were set or measured, but entropy was not. That will be the object of our following studies. The algorithms of obtaining entropy and adiabats are a little bit more complicated than for isoterms for example, because entropy can not be measured as a PIMC observable. So we have to solve differential equations derived from thermodynamics. Formally they give all information about the system since we know $E(\rho, T)$ and $P(\rho, T)$, but it is not trivial to get the numerical results. As it was mentioned, the lattice of calculation points in temperature and extremely in density must include close points in a large range that means much calculations. On the one hand we want to explore a wide range. On the other hand, the points must be close enough to allow the calculation of derivatives. We also plan to develop an alternative way of derivatives calculation based on constructing observables for them.

An other problem to be explored is to perform the thermalization from "liquid" to crystal solid state in order to determine the lower limit for the phase transition. We expect that it can be done much faster starting from two phase system.

6 Acknowledgements

The reported study was supported by the Supercomputing Center of Lomonosov Moscow State University [6].

This work was partially supported by The Ministry of education and science of Russian Federation (grant No.8376).

References

[1] J. Schneider, The Extrasolar Planets Encyclopedia: Interactive Extra-solar Planets Catalog http://exoplanet.eu/

[2] Bagenal, Fran Giant planet magnetospheres, In: Annual review of earth and planetary sciences. Vol. 20 (A93-45370 18-46), p. 289-328

[3] M. I. Eremets I. A. Troyan Conductive dense hydrogen DOI: 10.1038/NMAT3175

[4] Ceperley D M *Rev. Mod. Phys.* **67** 279 (1995)

[5] Militzer B, Graham R L *Journal of Physics and Chemistry of Solids* **67** 2136 (2006)

[6] Voevodin Vl.V., Zhumatiy S.A., Sobolev S.I., Antonov A.S., Bryzgalov P.A., Nikitenko D.A., Stefanov K.S., Voevodin Vad.V Practice of "Lomonosov" Supercomputer // Open Systems J. - Moscow: Open Systems Publ., 2012, no.7. [http://www.osp.ru/os/2012/07/13017641/] (In Russian)